Contents lists available at ScienceDirect

Physica Medica

journal homepage: www.elsevier.com/locate/ejmp

Image preprocessing to improve the accuracy and robustness of mutual-information-based automatic image registration in proton therapy

Kouta Hirotaki [a,b], Shunsuke Moriya [c,*], Tsunemichi Akita [b], Kazutoshi Yokoyama [b], Takeji Sakae [c]

[a] Doctoral Program in Medical Sciences, Graduate School of Comprehensive Human Sciences, University of Tsukuba, Ibaraki 3058577, Japan
[b] Department of Radiological Technology, National Cancer Center Hospital East, Chiba 2778577, Japan
[c] Faculty of Medicine, University of Tsukuba, Ibaraki 3058575, Japan

A B S T R A C T

Purpose: We propose a method that potentially improves the outcome of mutual-information-based automatic image registration by using the contrast enhancement filter (CEF).
Methods: Seventy-six pairs of two-dimensional X-ray images and digitally reconstructed radiographs for 20 head and neck and nine lung cancer patients were analyzed retrospectively. Automatic image registration was performed using the mutual-information-based algorithm in VeriSuite®. Images were preprocessed using the CEF in VeriSuite®. The correction vector for translation and rotation error was calculated and manual image registration was compared with automatic image registration, with and without CEF. In addition, the normalized mutual information (NMI) distribution between two-dimensional images was compared, with and without CEF.
Results: In the correction vector comparison between manual and automatic image registration, the average differences in translation error were < 1 mm in most cases in the head and neck region. The average differences in rotation error were 0.71 and 0.16 degrees without and with CEF, respectively, in the head and neck region; they were 2.67 and 1.64 degrees, respectively, in the chest region. When used with oblique projection, the average rotation error was 0.39 degrees with CEF. CEF improved the NMI by 17.9 % in head and neck images and 18.2 % in chest images.
Conclusions: CEF preprocessing improved the NMI and registration accuracy of mutual-information-based automatic image registration on the medical images. The proposed method achieved accuracy equivalent to that achieved by experienced therapists and it will significantly contribute to the standardization of image registration quality.

Introduction

In current radiotherapy, image-guided radiotherapy (IGRT) has been applied to achieve high-accuracy treatment [1,2]. Image registration for patient alignment is performed by the therapist's manual image registration or by automatic image registration. In manual image registration, the therapist specifies the translation (RL, AP, SI) and rotation (yaw, pitch, roll) error by visual evaluation, and uses the correction vector calculated from these errors to align the patient's position. However, manual image registration is problematic in that the registration accuracy differs depending on the therapist. Court et al., [3] reported an inter-observer uncertainty at the isocenter of 0.6–1.2 mm in translation error. Mechalakos et al., [4] reported an inter-observer

uncertainty in translation error of 1.0 mm, and an uncertainty in rotation error of 1.0 degree in the sagittal view and 1.5 degrees in the coronal view. In contrast, automatic image registration enables image registration to be performed with constant accuracy and speed and without dependence on the operator's skill [5,6]. The similarity required for automatic image registration is calculated using techniques such as cross-correlation, entropy, and mutual information (MI) [7–12]. In particular, MI is widely used in automatic image registration for medical images with different modalities, such as two-dimensional (2D) X-ray images and digitally reconstructed radiographs (DRRs) [13,14]. However, MI-based automatic image registration is not always sufficiently accurate and robust for clinical images.

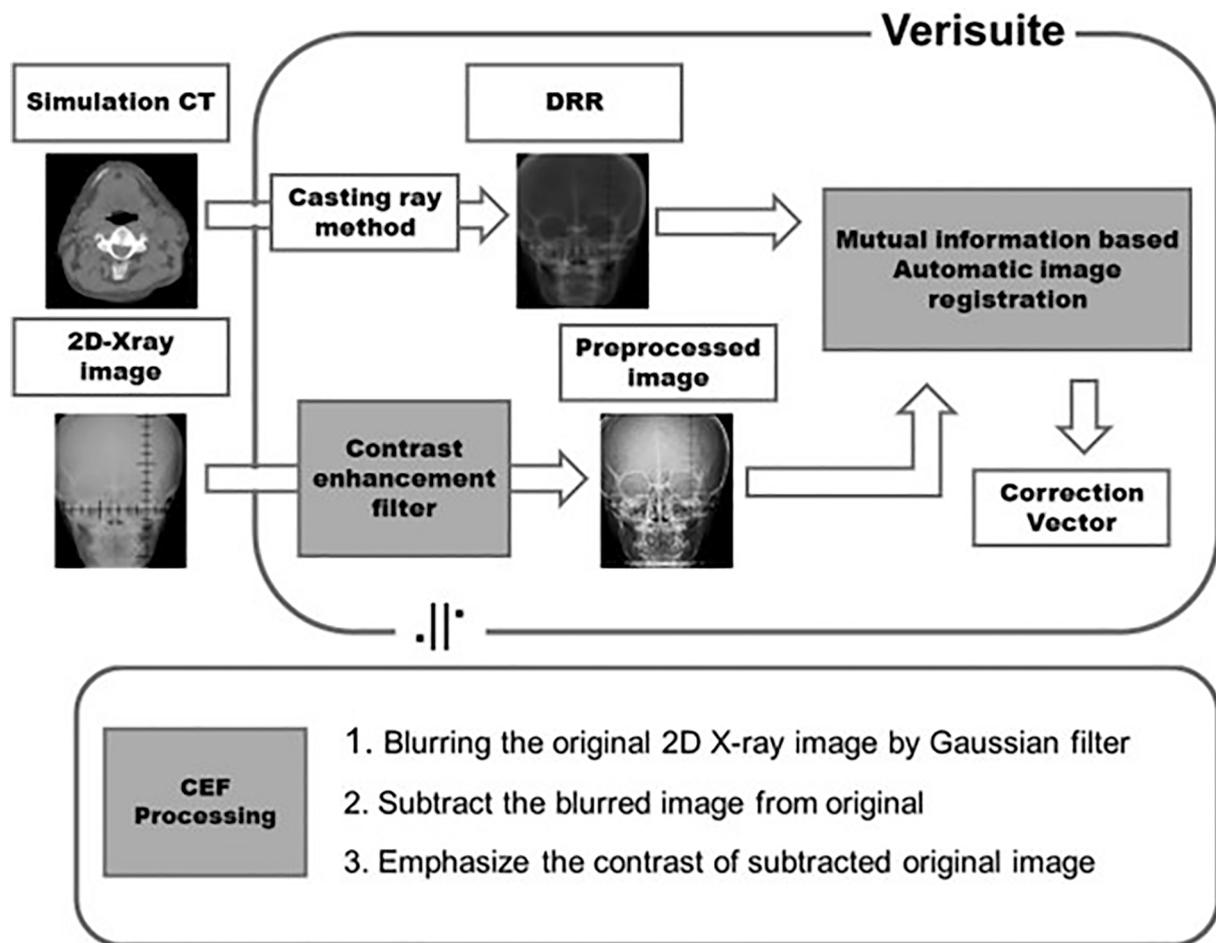In proton beam therapy (PBT), the range error affects the accuracy of

Fig. 1. Proposed 2D3D registration workflow with the contrast enhancement filter (CEF) for mutual-information-based automatic image registration.

the delivered dose distribution [15,16]. Therefore, daily treatment with PBT requires the positions of the anatomical structures at the time of planning to correspond exactly to those at the time of fraction delivery, with high accuracy. This is achieved by adopting IGRT—using 2D X-ray images and computed tomography (CT)—during daily PBT. Although either 2D X-ray, Cone beam CT (CBCT), or in-room CT images can be used for IGRT, in-room CT images are infrequently used because of their inefficiency in daily treatment, and CBCT is high radiation exposure to patients than 2D X-rays and may not be appropriate for daily IGRT [17]. 2D3D image registration is comparable to CT in accuracy of matching in head region [18]. Especially in the treatment of pediatric patients, high-speed workflow and reduction of radiation exposure by automatic 2D3D image registration are effective. Automatic 2D3D image registration uses 2D X-ray images and DRRs reconstructed from CT are employed for daily image registration [19]. However, MI-based automatic image registration alone cannot achieve patient alignment with sufficient accuracy for PBT treatment and the result must be corrected by the therapist's manual operation. Therefore, to improve the performance of automatic image registration, we examined a new procedure for MI-based automatic image registration using image preprocessing. The purpose of this study was to investigate the use of image preprocessing to achieve high accuracy and robustness using the existing MI-based automatic image registration algorithm. We evaluated the accuracy and robustness of image preprocessing by comparing the calculated correction vectors in automatic image registration with manual image registration.

Methods

Patient information and image dataset

Twenty patients with head and neck cancer and nine with lung cancer who were treated with PBT were selected for this retrospective study. The effectiveness of the proposed method was evaluated using 76 sets of images; each set comprised 2D X-ray images for the AP, LAT, and oblique dimensions, and the corresponding DRR image. The contents of the study, including the investigation procedure and the handling of patient information, were approved by the institutional review board (IRB) of the National Cancer Center Hospital East (IRB No. 2018–076).

The 2D X-ray images used in this study were acquired using an A-277 X-ray tube (Varian, USA) and the Paxscan 4030E flat panel detector (Varian, USA). The gantry angle used to obtain the 2D X-ray images was 0 degrees for the AP images, 270 degrees for the LAT images, and 35 degrees and 235 degrees for the oblique images. The source-to-isocenter distance was 1480 mm and the source-to-detector distance was 2150 mm. The image size was 3200 × 2304 pixels, and the pixel size was 0.127 mm. The scan parameters for the head and neck region were fixed at a voltage of 85 kVp, current of 400 mA, and scan time of 20 ms. The scan parameters for the lung region AP images were 120 kVp, 400 mA, and 16 ms; the parameters for the LAT images were 120 kVp, 400 mA, and 40 ms. However, the scan time was manually adjusted to optimize the effect of body thickness. The 2D X-ray images of the head and neck region were acquired at the isocenter location after correcting the position by using the described marker on the thermoplastic mask. The 2D X-ray images of the lung region were acquired after correcting the position by using the described marker on the skin surface. The 2D X-ray
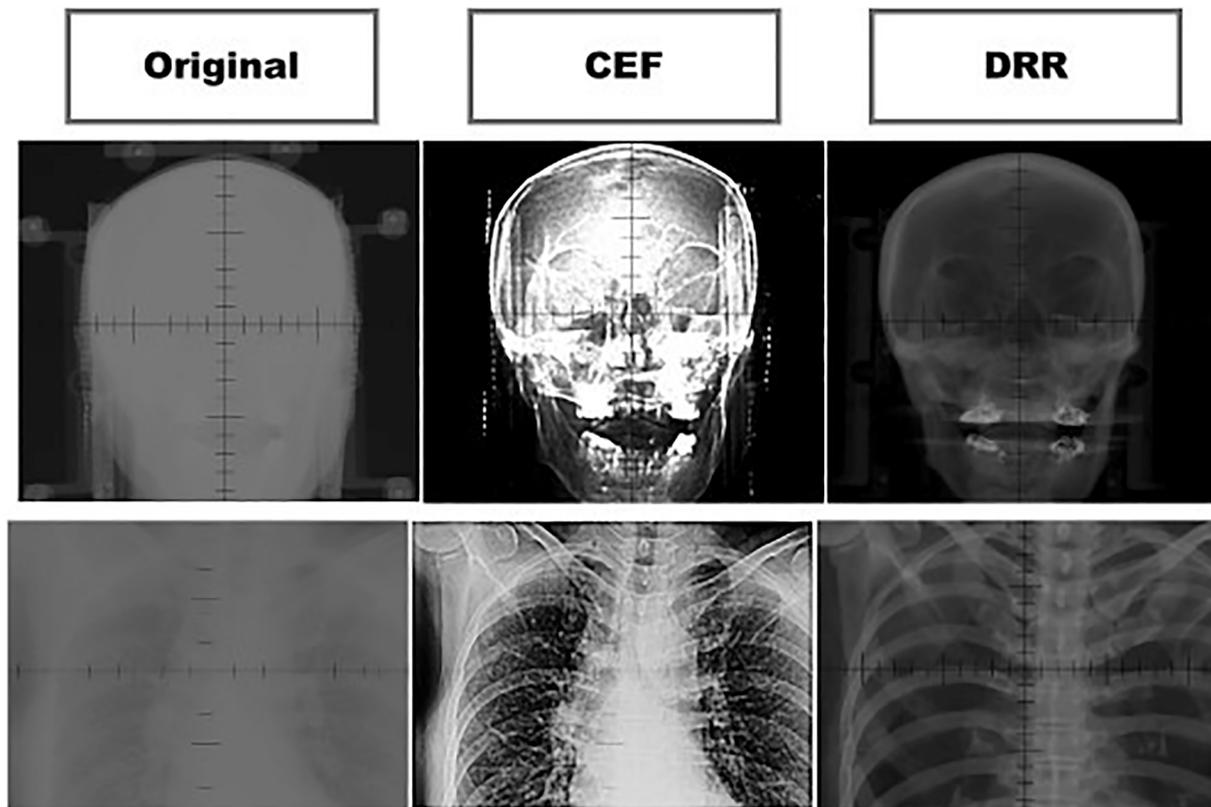
Fig. 2. (Left) Original image obtained by the imaging system under the reference scan parameters. (Center) Original image after processing by the contrast enhancement filter (CEF) in VeriSuite®. (Right) Digitally reconstructed radiograph (DRR) created from the simulation CT using the ray casting method.
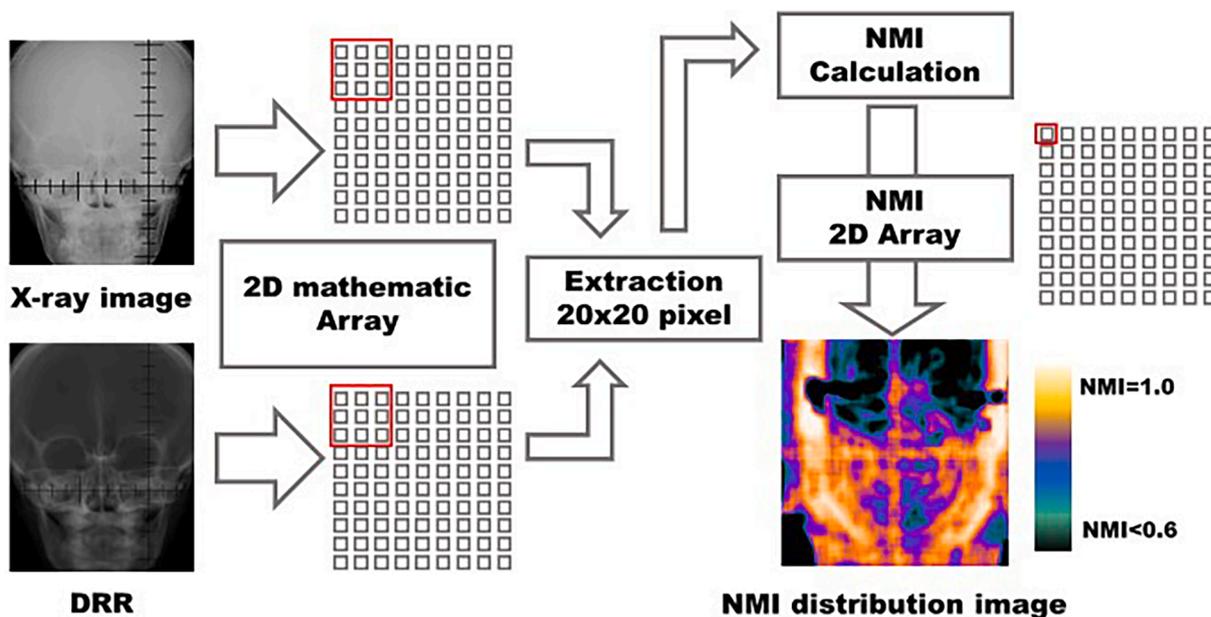

Fig. 3. Procedure to create the normalized mutual information (NMI) map.

images were captured daily during the treatment period and were captured again after correcting the position to check the final position of the patient before treatment. For nine lung cancer patients, either the AP and LAT combination or the diagonal image combination was selected at the therapist's discretion for each treatment day.

Image registration and Creating the DRR was performed the VeriSuite® (MedCom, Germany) [20]. This algorithm employs the ray

casting method for generate the DRR and the 2D3D registration method for image registration [21]. The simulation CT was acquired 1–2 weeks before treatment, and the rescan CT was scheduled by physicians as necessary. The scan parameters were as follows: the tube voltage was 120 kVp, the tube current used automatic exposure control with a standard deviation of 10 Hounsfield unit, the rotation speed was 0.5 cycle/s, the slice thickness was 1 mm. Helical scan was used for the head

Table 1

NMI between DRRs and 2D X-ray images (AP and LAT) for the 20 head and neck cases. The "CEF" and "Original" columns show results with and without CEF preprocessing, respectively.

Patient	NMI for AP image		NMI for LAT image	
	Original	CEF	Original	CEF
1	0.711	0.793	0.632	0.703
2	0.634	0.738	0.655	0.767
3	0.499	0.619	0.512	0.656
4	0.676	0.794	0.598	0.715
5	0.649	0.764	0.647	0.750
6	0.473	0.614	0.465	0.573
7	0.665	0.801	0.649	0.780
8	0.670	0.755	0.630	0.715
9	0.672	0.787	0.671	0.783
10	0.654	0.791	0.591	0.708
11	0.668	0.821	0.638	0.716
12	0.500	0.683	0.511	0.632
13	0.673	0.808	0.608	0.710
14	0.602	0.702	0.523	0.585
15	0.524	0.695	0.489	0.657
16	0.547	0.698	0.546	0.680
17	0.660	0.783	0.671	0.751
18	0.678	0.799	0.655	0.742
19	0.678	0.798	0.621	0.705
20	0.715	0.818	0.617	0.711
Average	0.63	0.75	0.60	0.70
SD	0.07	0.06	0.06	0.06

Table 2

NMI between DRRs and 2D X-ray images (AP and LAT) for the nine chest cases.

Patient	NMI for AP image		NMI for LAT image	
	Original	CEF	Original	CEF
1	0.639	0.778	0.583	0.701
2	0.621	0.761	0.580	0.710
3	0.694	0.777	0.646	0.690
4	0.693	0.775	0.612	0.715
5	0.444	0.616	0.427	0.567
6	0.475	0.618	0.470	0.568
7	0.700	0.796	0.690	0.795
8	0.692	0.784	0.705	0.728
9	0.612	0.784	0.581	0.748
Average	0.62	0.74	0.59	0.69
SD	0.09	0.07	0.09	0.07

Table 3

NMI between DRRs and oblique 2D X-ray images for the nine chest cases.

Patient	NMI for right oblique		NMI for left oblique	
	Original	CEF	Original	CEF
1	0.699	0.775	0.712	0.778
2	0.639	0.762	0.641	0.749
3	0.606	0.759	0.593	0.759
4	0.695	0.775	0.673	0.765
5	0.560	0.646	0.563	0.632
6	0.571	0.643	0.599	0.649
7	0.666	0.793	0.679	0.797
8	0.689	0.762	0.683	0.764
9	0.666	0.778	0.652	0.785
Average	0.64	0.74	0.64	0.74
SD	0.05	0.05	0.05	0.06

and neck, and non-helical scan with respiratory synchronization mode was used for the chest.

Image preprocessing

The discrepancy between the characteristics of DRRs and those of 2D X-ray images affects the registration accuracy and robustness of automatic image registration. These discrepancies are caused by anatomical changes in the medical images (i.e., the 2D X-ray images). This led us to consider preprocessing the 2D X-ray images to correct this discrepancy. Preprocessing suppresses the signal of the soft tissue that is affected by anatomical changes and emphasizes the contours of the bone structures. In this study, the contrast enhancement filter (CEF) in VeriSuite® was adopted for preprocessing (Fig. 1). This filter has two functions: the first is to suppresses image blur and sharpens contours, and the second is to reduce the background noise by subtracting the blurred original image from the original image itself. Fig. 2 shows the difference between the characteristics of the original images and those of the 2D X-ray images processed by CEF in the head and neck region and the chest region. This CEF preprocessing can be generalized using Gaussian filtering and contrast enhancement preprocessing in ImageJ [22]. Both methods (VeriSuite® and ImageJ) were evaluated in a preliminary study. While the NMI between the original image and the DRR was 0.57, in ImageJ, the NMI increased to 0.64 by subtracting the blurred image under the Gaussian filter processing from the original image. Furthermore, the NMI increased to 0.76 by adding the contrast enhancement processing. The NMI under the use of Medcom CEF was 0.67. Their performance, with respect to the improvement of the characteristics, was found to be similar.

Image registration accuracy and robustness

The image registration accuracy was evaluated by comparing the correction vector in automatic image registration with manual image registration. The correction vector was constructed from the translation factor (LR, SI, AP) and rotation factor (yaw, pitch, roll). Automatic image registration was performed on the original images and preprocessed images with CEF to obtain the correction vector between these images and the DRRs. The algorithm used for automatic image registration was based on MI, as adopted in VeriSuite®:

$$\mathrm{MI}(X,\ Y\ ) = \sum_{Y}\sum_{X} P(X,\ Y\ )\log_2 P(X,Y)/P(X)P(Y) \tag{1}$$

where P(X) and P(Y) represent the marginal probability functions for images X and Y (the 2D X-ray image and the DRR), respectively, and P(X, Y) represents their joint probability density function. Manual image registration was performed by a skilled therapist, and the position decided was checked by another therapist. The position error was obtained from the difference between the correction vectors of the automatic image registration and manual image registration as the ground truth. In addition, to evaluate the effectiveness of MI-based automatic image registration with CEF for clinical, manual operation was compared to CEF method. Manual image registration in clinical was performed by three therapists and one medical physicist, and position was decided as level of clinical uses. The robustness of image registration was evaluated using the invalid ratio, which was calculated as the number of unsuccessful automatic image registration cases divided by the number of cases used for measurement. To measure the invalid ratio, automatic image registration was performed after correcting the patient position using only the alignment on the RL, SI, and AP. We defined an "unsuccessful case" as one in which the translation error > 2.5 mm, and the rotation error > 3 degrees in any one of the correction vectors.

Normalized mutual information (NMI) distribution

The normalized mutual information (NMI) was calculated to evaluate the contribution of the proposed image preprocessing to the improvement of the image characteristics in MI-based automatic image registration. NMI is defined by the following equation:

$$\mathrm{NMI}(X,Y) = \mathrm{MI}(X,Y)/\sqrt{H(X)H(Y)} \tag{2}$$

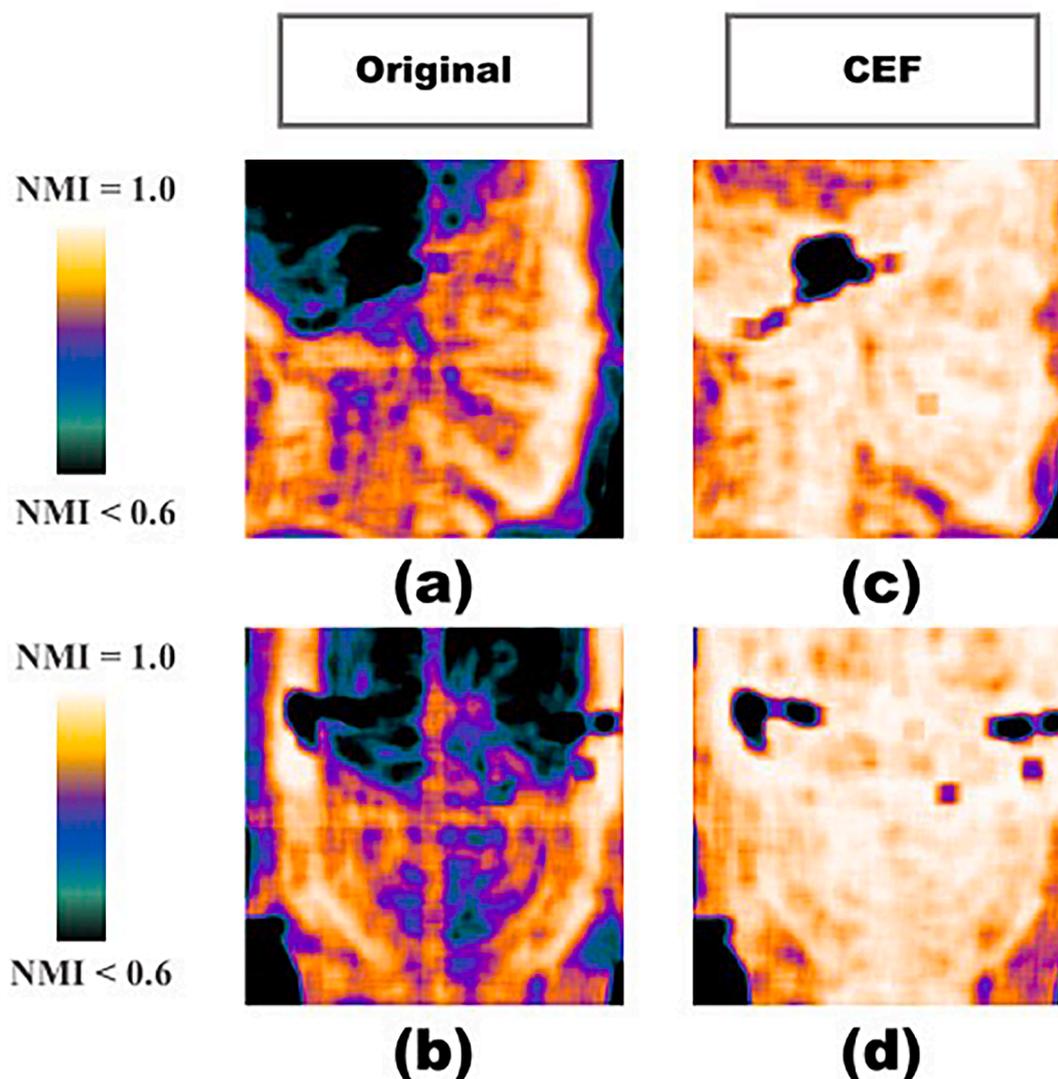where MI(X, Y) represents the MI between images X and Y (Eq. (1)), and

Fig. 4. NMI map for the AP and LAT images in the head and neck region. (a) Original LAT image. (b) Original AP image. (c) LAT image after preprocessing by contrast enhancement filter (CEF). (d) AP image after preprocessing by CEF. Color scale: white shows regions with NMI = 1.0 (maximum) and black shows regions with NMI < 0.6. The CEF-preprocessed images improved NMI in the location of sella turcica, occipital bone, mandible, cervical spine, and orbital bone.

H(X) and H(Y) represent the marginal entropies of images X and Y, respectively. In-house software (developed using Python) was used to calculate the NMI. The original 2D X-ray images and the preprocessed image were imported into the software, and each image was converted to a mathematical array. Each array was converted to a one-dimensional (1D) mathematical array for calculation, and the NMI value was obtained from these arrays.

To visualize the manner in which the MI-based algorithm performs image registration using anatomical structures, we presented the distribution of the NMI between a DRR and a 2D X-ray image in the form of an NMI map. This map was created using in-house software (developed using Python). Fig. 3 shows the procedure for creating the NMI map. The details of the procedure are as follows:

1. The 2D X-ray image and DRR are imported into the system and each image is converted to a 2D mathematical array.
2. One pixel is selected in the 2D X-ray image array, the corresponding pixel is selected in the DRR array, and 20 × 20 pixels are extracted around both of the selected pixels, as 2D arrays.
3. Each extracted 2D array is converted to a 1D mathematical array and the NMI is calculated using these arrays; in addition, new 2D arrays is created using these NMI values.

4. The data format of this array is converted to image format and the NMI map—with the NMI distribution expressed using color information—is displayed.

The NMI map that was created was displayed using the same window parameters to compare several conditions of the 2D X-ray images.

Manual and automatic image registration

To evaluate the effectiveness of MI-based automatic image registration with CEF, manual operation was compared to CEF method. Manual image registration was performed by three therapists and one medical physicist, and position was decided as level of clinical uses.

Results

Evaluation of NMI

Table 1 presents the NMI between the 2D X-ray image (with and without CEF) and the DRR for the 20 head and neck cancer patients. The average NMI values of the AP and LAT images without CEF were 0.63 ± 0.07 (mean $\pm$ SD) and 0.60 ± 0.06, respectively, and the average NMI
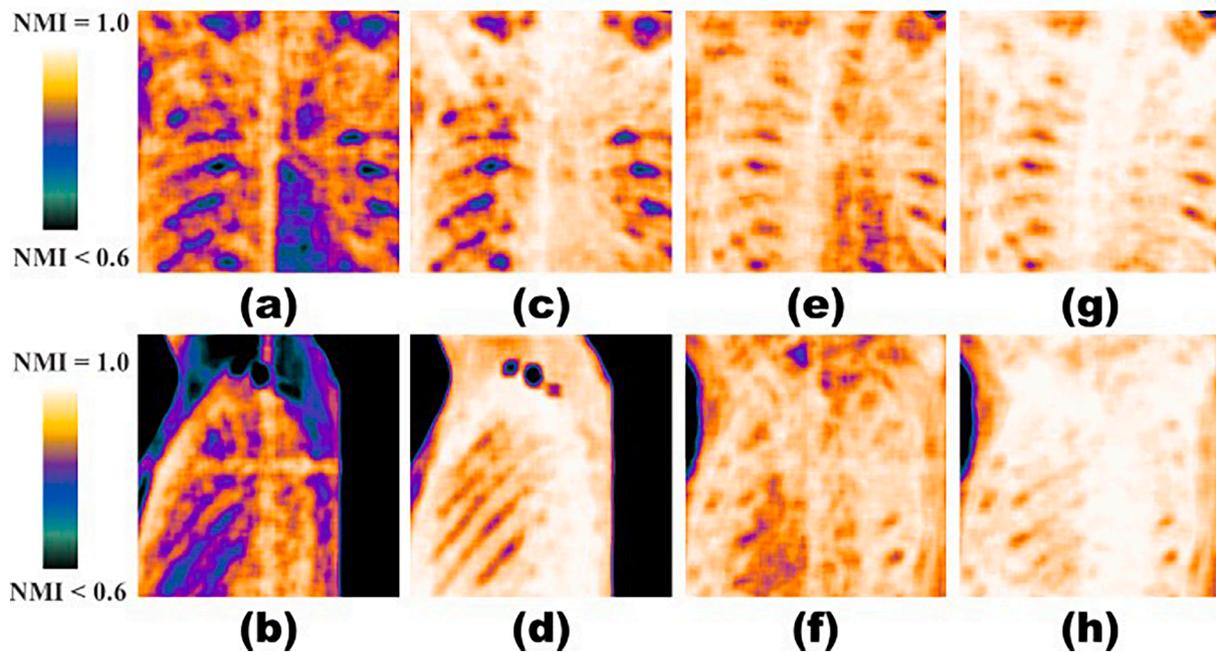
Fig. 5. NMI map for the AP, LAT, and oblique images in the chest region of patient no. 1. (a) Original AP image. (b) Original LAT image. (c) CEF-preprocessed AP image. (d) CEF-preprocessed LAT image. (e) Original right oblique image. (f) Original left oblique image. (g) CEF-preprocessed right oblique image. (h) CEF-preprocessed left oblique image. The corresponding NMI values are 0.639 (a), 0.583 (b), 0.778 (c), 0.701 (d), 0.699 (e), 0.712 (f), 0.775 (g), and 0.778 (h). The oblique images suppressed local low-NMI regions resulting from shoulder overlap, and the CEF-preprocessed images increased NMI in the thoracic spine, clavicle, and ribs.

Table 4
Difference of translation error and rotation error between automatic and manual image registration on the 20 head and neck cancer patients.

	Original	CEF
	Mean ± SD (Max)	Mean ± SD (Max)
R-L (mm)	0.81 ± 1.03 (3.95)	0.39 ± 0.33 (1.21)
S-I (mm)	0.65 ± 0.67 (2.24)	0.33 ± 0.25 (0.82)
A-P (mm)	0.48 ± 0.79 (3.10)	0.32 ± 0.25 (0.86)
Yaw (deg.)	0.70 ± 1.36 (5.58)	0.14 ± 0.13 (0.62)
Pitch (deg.)	0.59 ± 1.16 (4.86)	0.13 ± 0.08 (0.28)
Roll (deg.)	0.84 ± 1.10 (3.10)	0.21 ± 0.16 (0.6)

Table 5
Difference of translation error and rotation error between automatic and manual image registration, using AP, LAT, and oblique images, on the nine lung cancer cases.

	Original (AP/LAT)	CEF (AP/LAT)	Original (Oblique)	CEF (Oblique)
	Mean ± SD (Max)	Mean ± SD (Max)	Mean ± SD (Max)	Mean ± SD (Max)
R-L (mm)	1.12 ± 1.90 (3.63)	0.21 ± 0.37 (0.97)	0.14 ± 0.14 (0.50)	0.87 ± 0.71 (2.32)
S-I (mm)	1.67 ± 2.51 (7.09)	0.60 ± 1.34 (3.93)	0.64 ± 1.80 (5.37)	0.64 ± 0.71 (1.83)
A-P (mm)	1.01 ± 1.50 (3.18)	0.53 ± 0.94 (2.66)	0.19 ± 0.37 (1.09)	0.42 ± 0.59 (1.40)
Yaw (deg.)	2.58 ± 6.81 (20.01)	0.39 ± 0.58 (1.67)	1.10 ± 2.76 (8.03)	0.28 ± 0.39 (0.81)
Pitch (deg.)	3.70 ± 4.14 (11.87)	3.60 ± 7.41 (22.46)	1.60 ± 4.08 (12.25)	0.35 ± 0.47 (1.06)
Roll (deg.)	1.73 ± 2.07 (2.83)	0.94 ± 1.54 (3.22)	0.80 ± 0.99 (1.76)	0.53 ± 0.63 (1.16)

values of the AP and LAT images with CEF were 0.75 ± 0.06 and 0.70 ± 0.06, respectively. The use of CEF increased the NMI by 0.12 for the AP image and 0.10 for the LAT image. Table 2 presents the NMI between the 2D X-ray image (with and without CEF) and the DRR for the nine lung cancer patients. The average NMI values of the AP and LAT images without CEF were 0.62 ± 0.09 and 0.59 ± 0.09, respectively, and the average NMI values of the AP and LAT images with CEF were 0.74 ± 0.07 and 0.69 ± 0.07, respectively. The use of CEF increased the NMI by 0.12 for the AP image and 0.10 for the LAT image. The average NMI values of the right oblique and left oblique images without CEF were 0.64 ± 0.05 and 0.64 ± 0.05, respectively, and the average NMI values of the right oblique and left oblique images with CEF were 0.74 ± 0.05 and 0.74 ± 0.06, respectively (Table 3). The oblique image increased the average NMI by 0.02–0.05 and the SD by 0.04, compared with the AP and LAT images. The use of CEF increased the NMI by 0.1 for both left oblique and right oblique images.

NMI mapping was conducted for the head and neck images (AP and LAT) with and without CEF, the chest image (AP and LAT) with and without CEF, and the chest oblique image (right oblique and left oblique) with and without CEF. In the images of the head and neck region without CEF, high-NMI signals were observed for the mandible, forehead, nose tip, and occipital bone. However, regions with NMI < 0.6 were widely observed in the brain parenchyma. In contrast, in the images with CEF, although low-NMI signals were locally observed in the clivus, high-NMI signals were observed in most other regions (Fig. 4). These results indicate that the NMI distribution between the 2D X-ray images and the DRRs can be improved by using CEF preprocessing. In the images (AP and LAT) of the chest without CEF, areas with NMI < 0.6 were observed in the lung regions and shoulder overlapping regions, and the NMI values for the bone structure around the shoulder were low. In contrast, in the images with CEF, the NMI values of the bone structure increased in most regions but were suppressed in the low-NMI region in the shoulder. In the oblique images of the chest region without CEF, high-intensity (compared with the AP and LAT images) NMI signals were observed for the clavicle, rib, and sternum. In addition, in the oblique images with CEF, locally low-intensity NMI signals in the
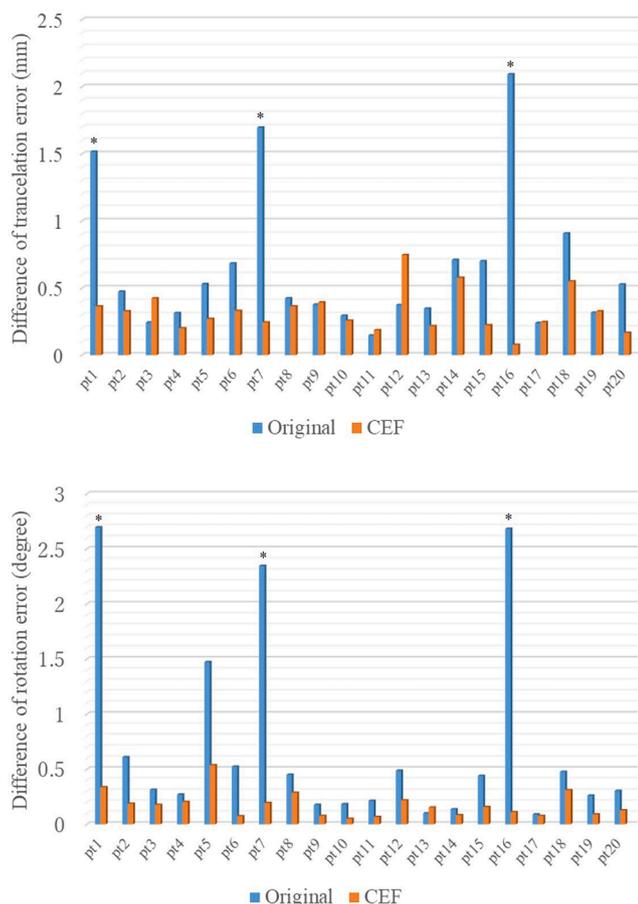
Fig. 6. The average difference of translation (upper) and rotation (lower) error between manual and automatic image registration with and without contrast enhancement filter (CEF), in head and neck region. The x-axis represents patient No., and the y-axis represents the difference of the correction vector. * Unsuccessful case (the translation error > 2.5 mm, and the rotation error > 3 degrees in any one of the correction vectors.).

Fig. 7. The average difference of translation (upper) and rotation (lower) error between manual and automatic image registration with and without contrast enhancement filter (CEF), in chest region. The x-axis represents patient No., and the y-axis represents the difference of the correction vector. * unsuccessful case (the translation error > 2.5 mm, and the rotation error > 3 degrees in any one of the correction vectors.).

shoulder region were removed and the NMI distribution was improved across the entire image (Fig. 5).

Translation and rotation error

The correction vectors in the automatic image registration for the original images and the CEF-preprocessed images were compared with the manual image registration (the ground truth). Tables 4 and 5 list the correction vector differences for translation (LR, SI, AP) and rotation (yaw, pitch, and roll) for the 40 head and neck images, 18 chest AP and LAT images, and 18 chest oblique images. In the average difference from manual image registration for the original image for the head and neck regions, the rotation errors (in degrees) were 0.70 ± 1.36 (mean ± SD) for yaw rotation, 0.59 ± 1.16 for pitch rotation, and 0.84 ± 1.10 for roll rotation. In contrast, in the CEF-preprocessed images, the rotation errors were 0.14 ± 0.13 for yaw rotation, 0.13 ± 0.08 for pitch rotation, and 0.21 ± 0.16 for roll rotation. CEF preprocessing reduced the yaw, pitch, and roll rotation errors, compared with the original images; in particular, for roll rotation, CEF preprocessing reduced the average error by 0.63 degrees and the SD by 0.94 degrees. In the average difference from manual image registration for the original image for the chest AP and LAT, the rotation errors were 2.58 ± 6.81 for yaw rotation, 3.70 ± 4.14 for pitch rotation, and 1.73 ± 2.07 for roll rotation. In contrast, in the CEF-preprocessed images, the rotation errors were 0.39 ± 0.58 for yaw rotation, 3.60 ± 7.41 for pitch rotation, and 0.94 ± 1.54 for roll rotation. The accuracy of the automatic image registration of the original
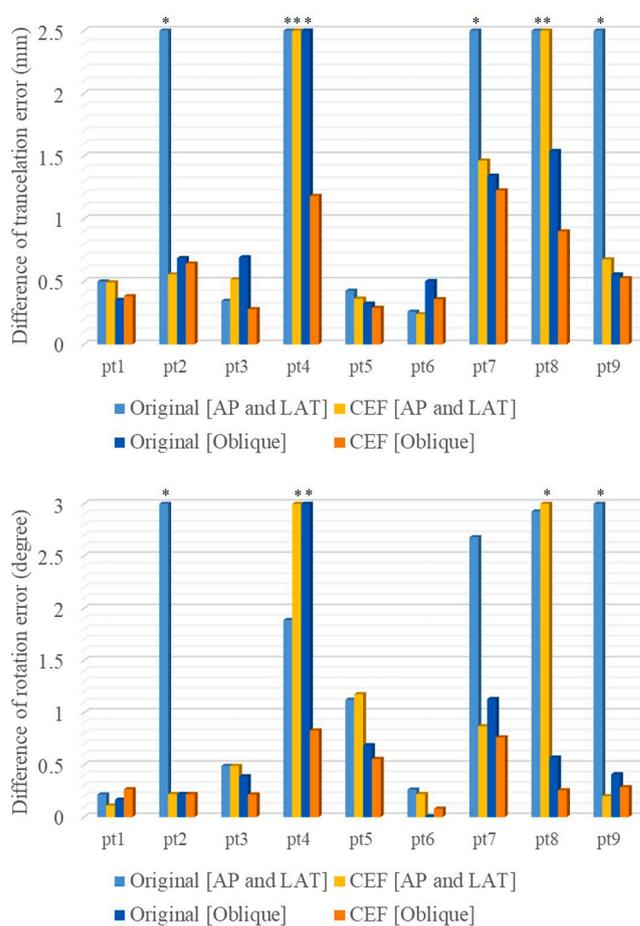
chest AP and LAT images tended to be inadequate, particularly for roll rotation, compared with that of the head and neck images. Although CEF preprocessing reduced the yaw and roll rotation errors, it did not contribute to improving the accuracy of pitch rotation. In the average difference from manual image registration for the CEF-preprocessed image of the chest oblique, the rotation errors were 0.28 ± 0.39 for yaw rotation, 0.35 ± 0.47 for pitch rotation, and 0.53 ± 0.63 for roll rotation. For the chest region, the rotation errors of the automatic image registration with CEF-preprocessed oblique images were the most reduced, compared with the orthogonal images with and without CEF and oblique images without CEF. Figs. 6 and 7 shows the average difference of translation and rotation error between manual and automatic image registration with and without CEF. In head and neck region, CEF preprocessing reduced the outlier cases and improved the rotation error. In chest region, the combination of Oblique image and CEF most reduced translation and rotation error.

In MI-based automatic image registration for the head and neck, the invalid ratio was 15 % without CEF and 0 % with CEF; for the chest region using AP and LAT images, it was 67 % without CEF and 22 % with CEF; for the chest region using oblique images, it was 11 % without CEF and 0 % with CEF. The number of invalid cases was small in head and neck images and chest oblique images. In contrast, the MI-based algorithm was ineffective for more than half of the chest AP and LAT images. The CEF method reduced the invalid ratio in all cases.
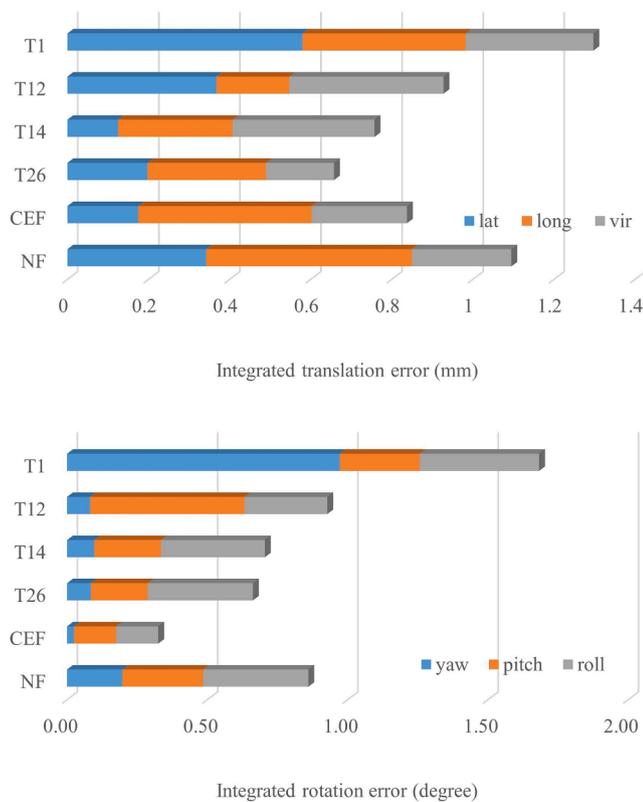
Fig. 8. The comparison of integrated translation error (upper) and rotation error (lower) error in the head region. * T: Therapist (the number represented their experience) †CEF: Automatic image registration with Contrast enhancement filter ‡NF: Automatic image registration without filter processing.

Manual operation vs automatic image registration with CEF

Comparison between manual operation by four therapists and MI-based automatic registration with CEF was shown Fig. 8. In the manual result, the accuracy of image registration varies depending on years of experience. and the difference with the grand trues was smaller for therapists with more years of experience. CEF method showed the best correction values in adjusting for rotation error.

Discussion

This study sought to improve the registration accuracy and robustness of MI-based automatic image registration using image preprocessing. The MI-based algorithm is widely used in clinical applications for image registration of DRRs and 2D X-ray images, and high registration accuracy has been confirmed in the phantom study. In this study, we performed image preprocessing to improve the automatic image registration accuracy and robustness for 2D3D image registration with an MI-based algorithm using clinical images, and evaluated the effectiveness of the proposed procedure and workflow. Image preprocessing was performed using blurring subtraction and contrast enhancement. The similarity between DRRs and 2D X-ray images was evaluated using NMI. Ranjbar et al., [23] assessed the similarity between fluoroscopic images and DRRs created from 4DCT using NMI. In that report, the NMI between 2D X-ray images and DRRs was shown to be 0.45–0.85 in five lung patients. Our analysis of nine lung patients showed that the NMI was 0.43–0.71 in orthogonal images; these findings are in agreement with [23]. Using the proposed CEF method, the NMI was 0.57–0.80 in lung patients. The proposed CEF method increased the NMI by 0.1 in all cases, demonstrating a large improvement compared with previous studies. In addition, we performed NMI mapping to visualize the

influence of image characteristics on MI-based automatic image registration. In the NMI map of the head and neck images without CEF, a region with NMI < 0.6 was observed in the brain parenchyma. In contrast, with CEF images, the NMI was increased in almost all regions. Although a local region with NMI < 0.6 was found in the clivus, it had no influence on the registration accuracy. In the chest region images without CEF, a region with NMI < 0.6 was observed over a wide area of the image. In oblique images with CEF, a large increase in NMI was observed. This was achieved by avoiding bone overlap by using oblique projection. As a result, oblique images with CEF achieved the best NMI distribution and the smallest difference in rotation errors (pitch and roll rotation), compared with manual operation. Hence, our CEF method with oblique images may be an effective strategy in MI-based automatic image registration for the chest region. These contributions to accuracy are attributed to the effect of CEF preprocessing on reducing the difference in image characteristics between DRRs and 2D X-ray images.

Williams et al., [12] investigated the accuracy and robustness of registration for human skulls using several image registration algorithms. They reported a translation error of 2.34 mm and a rotation error of 0.63 degrees when using MI-based automatic image registration. Gendrin et al., [24] reported that, in an evaluation of registration accuracy for a porcine cadaver head, MI-based algorithms were more accurate than other intensity-based methods, with a target registration error between a DRR and a 2D X-ray image of 2.20 ± 0.92 mm (mean ± SD). This result is not sufficiently accurate for daily patient alignment in PBT. Using the proposed method, in the head and neck region, the difference between automatic image registration with CEF and manual image registration was < 1 mm for the translation error, and yaw = 0.14, pitch = 0.13, and roll = 0.21 for the rotation error. The proposed method is inferior to the current method in some translation and rotation errors for patients 3 and 13. Patient No. 3 is a patient with a therapeutic device implanted in the brain. This device is distinctive, it improved mutual information and registration accuracy in the non-CEF images. Patient No. 13 is a patient with nasal cancer. Isocenter located nasal center and lacks the occipital information from registration image. It affected the accuracy of proposed method. However, inferior status was small and either translation or rotation error was superior to the non-filter method. In a comparison of the required time to perform image registration, the mean time for manual image registration (in the head and neck region) by four therapists was 2 min, whereas the time for automatic image registration with CEF was 15 s. The proposed CEF procedure facilitates high accuracy and fast treatment, and is dramatically effective in the head and neck region. In the comparison with 3D imaging, although in-room CT or CBCT is used to observe changes in body thickness and tumor size for adaptive treatment, these variations can be also detected using 2D X-ray images [25]. In addition, this method is faster than In-room CT process, and it is lower exposure to patients than CBCT process. Especially, the proposed procedure will be useful for suppressing intra-fractional motion and reducing exposure dose in pediatric treatment.

This study had several limitations. The algorithms for automatic image registration and CEF preprocessing used in the study were provided by VeriSuite®. The registration algorithm is based on MI and uses CEF to subtract the Gaussian blurring image from the original and emphasize the image contrast. Although the function of CEF can be reproduced in ImageJ, part of the MI-based automatic image registration algorithm was not revealed, and it may not be possible to reproduce the results of this study when using different automatic image registration systems. In addition, although manual image registration by two experienced therapists were used as the ground truth, the results may vary according to the therapists' policy.

Conclusions

We investigated image preprocessing to improve the accuracy and robustness of MI-based automatic image registration. The proposed

method using CEF achieved high accuracy and robustness, compared with the conventional method without CEF. The use of CEF pre-processing increased the NMI for the head and neck region and the chest region. Furthermore, we visualized the difference in image characteristics between DRRs and 2D X-ray images by performing NMI mapping. NMI mapping revealed the effectiveness of CEF preprocessing on the performance of MI-based automatic image registration and the effectiveness of oblique projection on automatic image registration in the chest region. The incorporation of CEF preprocessing in the automatic image registration procedure is expected to improve the accuracy and robustness of MI-based automatic image registration on clinical images. It may also be useful for reducing the time necessary for image registration and the differences between therapists with respect to registration accuracy.

Declaration of Competing Interest

The authors declare that they have no known competing financial interests or personal relationships that could have appeared to influence the work reported in this paper.

References

[1] Court LE, Wolfsberger L, Allen AM, James S, Tishler RB. Clinical experience of the importance of daily portal imaging for head and neck IMRT treatments. J Appl Clin Med Phys 2008;9:26–33. https://doi.org/10.1120/jacmp.v9i3.2756.
[2] Kang H, Lovelock DM, Yorke ED, Kriminski S, Lee N, Amols HI. Accurate positioning for head and neck cancer patients using 2D and 3D image guidance. J Appl Clin Med Phys 2011;12:86–96. https://doi.org/10.1120/jacmp.v12i1.3270.
[3] Court LE, Allen A, Tishler R. Evaluation of the precision of portal-image-guided head-and-neck localization: An intra- and interobserver study. Med Phys 2007;34:2704–7. https://doi.org/10.1118/1.2747050.
[4] Mechalakos JG, Hunt MA, Lee NY, Hong LX, Ling CC, Amols HI. Using an onboard kilovoltage imager to measure setup deviation in intensity-modulated radiation therapy for head-and-neck patients. J Appl Clin Med Phys 2007;8:28–44. https://doi.org/10.1120/jacmp.v8i4.2439.
[5] Wu J, Su Z, Li Z. A neural network-based 2D/3D image registration quality evaluator for pediatric patient setup in external beam radiotherapy. Journal of Applied Clinical Medical Physics 2016;17(1):22–33.
[6] Yoon M, Cheong M, Kim J, Shin DH, Park SY, Lee SB. Accuracy of an automatic patient-positioning system based on the correlation of two edge images in radiotherapy. J Digit Imaging 2011;24:322–30. https://doi.org/10.1007/s10278-009-9269-6.
[7] Munbodh R, Jaffray DA, Moseley DJ, Chen Z, Knisely JPS, Cathier P, et al. Automated 2D–3D registration of a radiograph and a cone beam CT using line-segment enhancement. Med Phys 2006;33:1398–411. https://doi.org/10.1118/1.2192621.
[8] Penney GP, Weese J, Little JA, Desmedt P, Hill DLG, Hawkes DJ. A comparison of similarity measures for use in 2D–3D medical image registration. IEEE T Med Imaging 1998;17:586–95. https://doi.org/10.1109/42.730403.
[9] Russakoff DB, Rohlfing T, Mori K, Rueckert D, Ho A, Adler JR, et al. Fast generation of digitally reconstructed radiographs using attenuation fields with application to 2D–3D image registration. IEEE T Med Imaging 2005;24(11):1441–54.
[10] Sawada A, Yoda K, Numano M, Futami Y, Yamashita H, Murayama S, et al. Patient positioning method based on binary image correlation between two edge images for proton-beam radiation therapy. Med Phys 2005;32:3106–11. https://doi.org/10.1118/1.2042247.
[11] Song G, Han J, Zhao Y, Wang Z, Du H. A review on medical image registration as an optimization problem. Curr Med Imaging Rev 2017;13:274–83. https://doi.org/10.2174/1573405612666160920123955.
[12] Williams KM, Schulte RW, Schubert KE, Wroe AJ. Evaluation of mathematical algorithms for automatic patient alignment in radiosurgery. Technol Cancer Res T 2015;14:326–33. https://doi.org/10.1177/1533034614547458.
[13] Maes F, Vandermeulen D, Suetens P. Medical image registration using mutual information. P IEEE 2003;91:1699–722. https://doi.org/10.1109/JPROC.2003.817864.
[14] Li G, Yang TJ, Furtado H, Birkfellner W, Ballangrud Å, Powell SN, et al. Clinical Assessment of 2D/3D Registration Accuracy in 4 Major Anatomic Sites Using On-Board 2D Kilovoltage Images for 6D Patient Setup. Technol Cancer Res Treat 2015;14(3):305–14. https://doi.org/10.1177/1533034614547444.
[15] Simone CB, Ly D, Dan TD, Ondos J, Ning H, Belard A, et al. Comparison of intensity-modulated radiotherapy, adaptive radiotherapy, proton radiotherapy, and adaptive proton radiotherapy for treatment of locally advanced head and neck cancer. Radiother Oncol 2011;101(3):376–82.
[16] Czerska K, Emert F, Kopec R, Langen K, McClelland JR, Meijers A, et al. Clinical practice vs. state-of-the-art research and future visions: Report on the 4D treatment planning workshop for particle therapy – Edition 2018 and 2019. Physica Med 2021;82:54–63.
[17] Ding GX, Alaei P, Curran B, Flynn R, Gossman M, Mackie TR, et al. Image guidance doses delivered during radiotherapy: Quantification, management, and reduction: Report of the AAPM Therapy Physics Committee Task Group 180. Med Phys 2018;45(5):e84–99. https://doi.org/10.1002/mp.12824.
[18] Zhao LR, Zhou YB, Li GH, Li QM, Yang DQ, Li HX, et al. The clinical feasibility and performance of an orthogonal X-ray imaging system for image-guided radiotherapy in nasopharyngeal cancer patients: Comparison with cone-beam CT. Phys Med 2016;32(1):266–71. https://doi.org/10.1016/j.ejmp.2015.11.010.
[19] Chou CR, Frederick B, Mageras G, Chang S, Pizer S. 2D/3D image registration using regression learning. Comput Vis Image Und 2013;117:1095–106. https://doi.org/10.1016/j.cviu.2013.02.009.
[20] B. P. Selby, G. Sakas, S. Walter, W.-D. Groch, U. Stilla. Selective X-Ray Reconstruction and Registration for Pose Estimation in 6 Degrees of Freedom, https://www.isprs.org/proceedings/XXXVII/congress/5_pdf/141.pdf.
[21] Fu D, Kuduvalli G. A fast, accurate, and automatic 2D-3D image registration for image-guided cranial radiosurgery: 2D-3D image registration for image-guided cranial radiosurgery. Med Phys 2008;35(5):2180–94.
[22] Rasband, W.S., ImageJ, U. S. National Institutes of Health, Bethesda, Maryland, USA, http://rsb.info.nih.gov/ij/, 1997-2012.
[23] Ranjbar M, Sabouri P, Mossahebi S, Sawant A, Mohindra P, Lasio G, et al. Validation of a CT-based motion model with in-situ fluoroscopy for lung surface deformation estimation. Phys Med Biol 2021;66:045035. 10.1088/1361-6560/abcbcf.
[24] Gendrin C, Markelj P, Pawiro SA, Spoerk J, Bloch C, Weber C, et al. Validation for 2D/3D registration II: The comparison of intensity- and gradient-based merit functions using a new gold standard data set. Med Phys 2011;38(3):1491–502.
[25] Hirotaki K, Moriya S, Tachibana H, Sakae T. Detection of anatomical changes using two-dimensional x-ray images for head and neck adaptive radiotherapy. Med Phys 2022;49:3288–97. https://doi.org/10.1002/mp.15587.